Available online at www.sciencedirect.com

ScienceDirect

Ceramics International 40 (2014) 1789–1796

CERAMICS INTERNATIONAL

www.elsevier.com/locate/ceramint

Preparation of 3D interconnected macroporous hydroxyapatite scaffolds by PVA assisted foaming method

Wei Wang[a], Baoshuai Chu[b], Chunqing Lin[b], Si Chen[b], Hongqiang Ru[b,*], Xinyan Yue[a], Quanli Jia[c,*]

[a]*Key Laboratory for Anisotropy and Texture of Materials of Ministry of Education (ATM), Northeastern University, Shenyang, PR China*
[b]*School of Materials and Metallurgy, Northeastern University, Shenyang, PR China*
[c]*School of Materials Science and Engineering, Zhengzhou University, 75 Daxue Road, Zhengzhou, PR China*

Received 2 June 2013; received in revised form 7 July 2013; accepted 16 July 2013
Available online 3 August 2013

Abstract

In this work, a simple method, called PVA assisted foaming method (PAF method), is for the first time reported to prepare 3D interconnected macroporous hydroxyapatite scaffolds (MHSs) without resorting to either porogens or templates or complicated chemical process. In this method, PVA-cryogels formed upon freezing is employed to set the air bubbles incorporated by the physical agitation and therefore the macroporous structures. After sintering, uniform and tuneable macropores in sizes of 90–130 μm with window pore sizes ranging from 20 to 70 μm can be facilely achieved. Moreover, balanced macroporosity (70–73%) and compressive strength of 1.8–3.1 MPa make the resultant MHSs promising materials for bone tissue engineering application. Simple modifications to this PAF method, *e.g.* applying an extra mechanical stirring or adding small amounts of surfactant (*e.g.* SDS) to PVA solution, enable further manipulation of the macroporous structures.

Keywords: B. Porosity; C. Strength; D. Apatite

1. Introduction

Hydroxyapatite (HA), the main mineral component of natural bone, has received extensive attention for bone repair or replacement in area of tissue engineering due to its excellent osteoconduction, overall safety and bone bonding ability with surrounding tissue [1–4]. So far, among many forms of HA bioceramics developed to fulfill various clinical requirements, such as granular [5], bulk [6,7] and porous forms [4,8], macroporous HA scaffolds (MHSs) with high porosity and three dimensional (3D) interconnectivity have been regarded as the most attractive bone substitutes. Especially, the porous structures of MHSs, mimicking those of natural bone, are expected to be beneficial to nutrient transfer, osteoconduction, metabolite elimination, cell migration and bone ingrowth, etc [9,10].

Optimal pore sizes for osteoconduction and bone ingrowth for biomaterials have rarely been defined and the intervals mentioned are quite variable in different studies. Some results in the literatures are even contradictory. For example, some studies reported that notable bone ingrowth occurred in pores smaller than 100 μm [11,12]; some authors considered that only pores larger than 100–150 μm can facilitate the ingrowth of mineralized bone [13–15]. Regardless of these discrepancies, it is generally accepted that the macropore sizes should fall in the range of 50–400 μm considering the applied cell size and the specific surface area for the availability of binding sites [16–18]. Therefore, the fabrication of MHSs with interconnected macropores with sizes fallen in above range should be highly desirable for the application.

With respect to the methods to prepare interconnected MHSs, so far there are mainly several kinds of methods involving (A) surfactant assisted foaming [19–22], (B) porogens [23–26], (C) macroporous perform/templates, *i.e.* sponges [27–29] and (D) chemical foaming agents [30,31], etc. In method A, as reported by Montufar et al. [20], foamed HA slips assisted by nonionic polysorbate 80 can be set through the hydrolysis of a-TCP to a calcium-deficient hydroxyapatite and eventually macroporous hydroxyapatite solid foam. Under the same principle but in different ways, the setting of the foamed slurry can be accomplished *via* a catalyzed sol–gel

*Corresponding authors. Tel./fax: +86 24 8368 0248.
E-mail addresses: ruhq@smm.neu.edu.cn (H. Ru), jiaquanli@zzu.edu.cn (Q. Jia)

0272-8842/$ - see front matter © 2013 Published by Elsevier Ltd and Techna Group S.r.l.
http://dx.doi.org/10.1016/j.ceramint.2013.07.079

process [19] or gel-casting process [22]. In method B, Tadic et al. [23] reported the fabrication of MHS using dual templates: with macropores templated by NaCl granules and interconnecting pores (windows) afforded by PVA fibers, both of which can be removed by water. Other porogens like sucrose granules, polymer spheres, oil droplets were often used to template the HA compact to form macropores [23–26]. In Method C, copying the macroporous structure of the sponges by coating or multi-coating HA-containing slurry is another option to prepare MHS [27–29], while the method D depends on the careful control over the chemical foaming process to obtain MHS with interconnected pores [30,31].

In abovementioned methods, either porogens/templates or chemical processes are employed, which could add the costs or complication to the fabrication process of MHS. This paper reports a recently patented method [32], called PVA assisted foaming method (denoted as PAF method), to fabricate MHS without using any porogens or templates or involving controlled chemical process. The principle of the PAF method is based on the cryogel characteristics of PVA in water and the incorporation of air bubbles by physical agitation. *Via* this method, MHSs with desirable 3D-interconnected porous structures and macropore sizes can be facilely obtained.

2. Materials and methods

2.1. Materials

Chemicals including $Ca(OH)_2$, $NH_3 \cdot H_2O$, H_3PO_4, c-HCl (37%) (AR grade), sodium dodecyl sulfate (SDS) and absolute ethanol were purchased from Sinopharm Chemical Reagent Co., Ltd. PVA (#2099, M_w ~90000) was purchased from Shanxi Sanwei Group Co. LTD. All the chemicals were used as received.

2.2. Preparation of HA powders

The preparation method of HA was similar to that reported previously [6] with slight modification. Briefly, the $Ca(OH)_2$ suspension was dispersed in water by vigorous stirring at 40 °C, to which the H_3PO_4 was added dropwise to produce a milky suspension. The pH value of the solution was then adjusted to 10.5 by using ammonia. The stirring was continued for another 6 h, followed by aging for 24 h at ambient temperature. The obtained precipitation was subject to centrifuging, washing, drying and finally calcination at 750 °C for 2 h in the air. After calcination, the powders were then ball-milled for 24 h in ethanol medium to break down agglomerates.

2.3. Preparation of MHSs by PAF method

Appropriate amounts of HA powders were added to the PVA aqueous solution (6.75 wt%) with pH value being adjusted from 7 to ~5 using a few drops of c-HCl in a polypropylene bottle. The incorporation of air bubbles was completed by vigorous shaking of the bottle with alumina balls for 20 min. The homogeneous HA slurry in PVA solution containing bubbles was transferred to an Al cup, and then put in a fridge set at −17 °C. After freezing at this temperature for 15 h, the sample was allowed to thaw at room temperature. The water in the gel was then extracted by immersing in ethanol for 5 h at room temperature. The extraction process was performed twice. The PVA/HA foam was dried at 120 °C for 5 h and calcined at 1250 °C for 2 h with heating ramp of 5 °C/min in the air. Obtained MHSs were denoted as PAFxx, where xx denotes the PVA/HA weight ratio.

For samples prepared with bubbles incorporated by extra stirring at 1200 rpm for 10 min, the stirring step was inserted after the shaking but before being transferred for freezing. The rest procedures are the same as the above. Obtained MHSs with extra stirring were denoted as PAFxx-R.

For samples using surfactant, *i.e.* SDS, to assist the foaming process, the surfactant was dissolved in the PVA solution before the addition of HA powders. In this work, SDS weight contents in PVA solution of 0.7‰ and 1.4‰ were studied. The rest procedures are the same as the above. Obtained MHSs using SDS were denoted as PAFxx-Syy, where 'xx' denotes the same, 'yy' means the concentrations of SDS (‰), *i.e.*, 0.7 or 1.4, in the PVA solution.

2.4. Characterization

The densities of sintered samples were measured *via* Archimedes principle using distilled water, and the porosity was calculated. The microstructure was examined using a scanning electron microscope (SEM, SSX-550) and the confocal laser scanning microscope (CLSM, OLS3100). The macropore size and its distribution were calculated based on the measured pore sizes in SEM images. The HA particle size was measured by using laser particle size analyzer (LA-920, Horida) using refractive index value of 1.6. The phase and crystallinity were analyzed via X-ray diffraction (XRD, Bruker D8) using Cu Ka radiation at 40 kV and 30 mA. The average crystallite size of the obtained HA was estimated by using the simple Scherrer equation: $D = k\lambda/(\beta\cos(\theta))$. The compressive strength of macroporous HAs (4–6 mm (in height) × 10 mm × 10 mm) was tested on a mechanical tester (WE-10A) at a crosshead speed of 0.5 mm/min. Five scaffolds were used to determine the average maximum compressive strength.

3. Results and discussion

3.1. HA powders

Firstly, the prepared HA powders were studied. The morphology of the synthesized HA powders after calcination at 750 °C for 2 h is shown in Fig. 1a. The obtained HA particles are uniform in sizes of about 100 nm. XRD analysis (Fig. 1b) reveals that the obtained HA powders by the precipitation are quite pure, evidenced by the non-existence of peaks from other phases compared with the reference XRD pattern. By careful examination of the XRD pattern of HA, some broadening in XRD peaks can be seen. The HA crystal sizes are estimated to be about 60 nm based on the Scherrer equation, which is consistent with the SEM result.

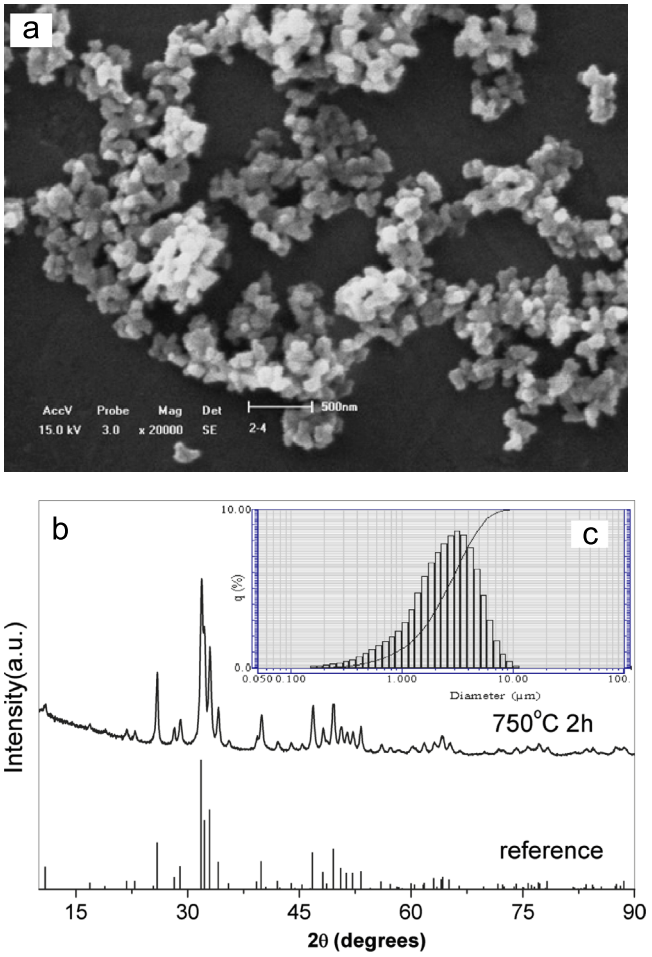

Fig. 1. SEM image (a), XRD pattern (b) and particle size distributions (c) of synthesized HA powders calcined at 750 °C for 2 h. The reference pattern (JCPDS 084-1998) of synthesized HA was also given for comparison purpose.

In addition, the HA powders tend to agglomerate to form secondary particles. After ball-milling, the measured particle size distributions obtained by laser particle size analyzer are shown in Fig. 1c, which gives the mean secondary particle size of about 2.9 μm.

3.2. 3D interconnected macroporous HA scaffolds

To prepare the MHS, the first step is to mix the HA powders with PVA solution. The formed slurry is subject to vigorous shaking for about 20 min. This process ensures the formation of both homogeneous slurry and incorporation of a large numbers of air bubbles. The effects of synthetic variables, such as PVA:HA weight ratio, extra mechanical stirring and surfactant on the macroporous structures of MHS were studied.

The influence of PVA:HA weight ratios on the macroporous structures of MHS is illustrated in Fig. 2. It can be seen that highly macroporous 3D-interconnected MHS can be successfully prepared by the PAF method irrespectively of the PVA:HA weight ratios. Both the SEM results and CLSM results correlate well with each other. High (Fig. 2a) or low (Fig. 2d) PVA:HA ratio leads to MHSs with less uniform macropores. The PAF4.9 and PAF4.4 show rather uniform macropores interconnected with each other, which can be seen from both SEM and CLSM measurements. The most probable primary macropore sizes for both PAF4.9 and PAF4.4 are around 130 μm, with the latter showing narrower pore size distributions. The interconnecting pores (windows) with sizes ranging from 20 μm to 60 μm are discernable in both cases. No doubts that the higher amounts of HA are added, the higher the viscosity of the slurry will be. As can be seen in PAF4.1 (Fig. 2d), high amounts of the HA added to the PVA solution result in inhomogeneous incorporation of air bubbles under the same physical agitation conditions and eventually non-uniform macropores. In the case of PAF5.5 with too less of HA, though the low viscosity allows the incorporation of high amounts of air bubbles, the merging of these bubbles also becomes more prominent, which can be seen from the larger and more interconnecting pores (30–70 μm, Fig. 2a). The most probable primary macropore size of PAF5.5 is about 90 μm, which is lower than those of PAF4.9 and PAF4.4 due to the emulsifying effect of increasing amounts of the PVA.

The mechanism to set the generated air bubbles in the PAF method is based on the cryogel characteristic of the PVA aqueous solution upon freezing, as shown in the Scheme 1. It has been extensively studied that the gelation of PVA in aqueous solution takes place *via* extensive inter-/intramolecular hydrogen bonds in forms of H···O···H in PVA during the freezing–thawing process [33]. After mixing physically, HA particles were homogeneously dispersed in the PVA solution to form slurry templated by a larger numbers of air bubbles, which will form the macropores. The contacting points of air bubbles form the interconnection of macropores (window pores). After freezing–thawing, the above macroporous structure will be set with the PVA/HA composite forming the walls, leaving water and air to occupy prior air bubbles. Therefore, the setting process based on the physical cryogel characteristic of PVA in water in the PAF method is significantly different from those relying on both the chemical process and surfactant [19,20,22]. In many works to prepare dried cryogels, the freeze drying process is often needed [33,34], which is time-consuming and needs a freeze dryer. In our case, water in the wet cryogels was extracted in ethanol by making use of the insolubility of PVA in ethanol. The following drying process can be accomplished easily in oven with nearly unchanged shape inherited from the container and negligible shrinkages (Fig. S1, Supplementary Data). If the wet PVA/HA cryogel composite is directly dried in the oven, distortion in shapes and diminishment in the porosity will take place due to the re-dissolving of PVA in water and the depletion of air bubbles even at temperature of as low as 50 °C. After extraction and drying in oven, the porous PVA/HA composite can be obtained with set macroporous structures. It is worthy to note that the homogeneously dispersed HA particles in PVA/HA composite are bound well by PVA molecules, which can be seen from the clear water/ethanol solution after extraction. After sintering, the joining of HA particles forms the wall with macroporous structure preserved and concomitant shrinkage in volume (Fig. S1, Supplementary

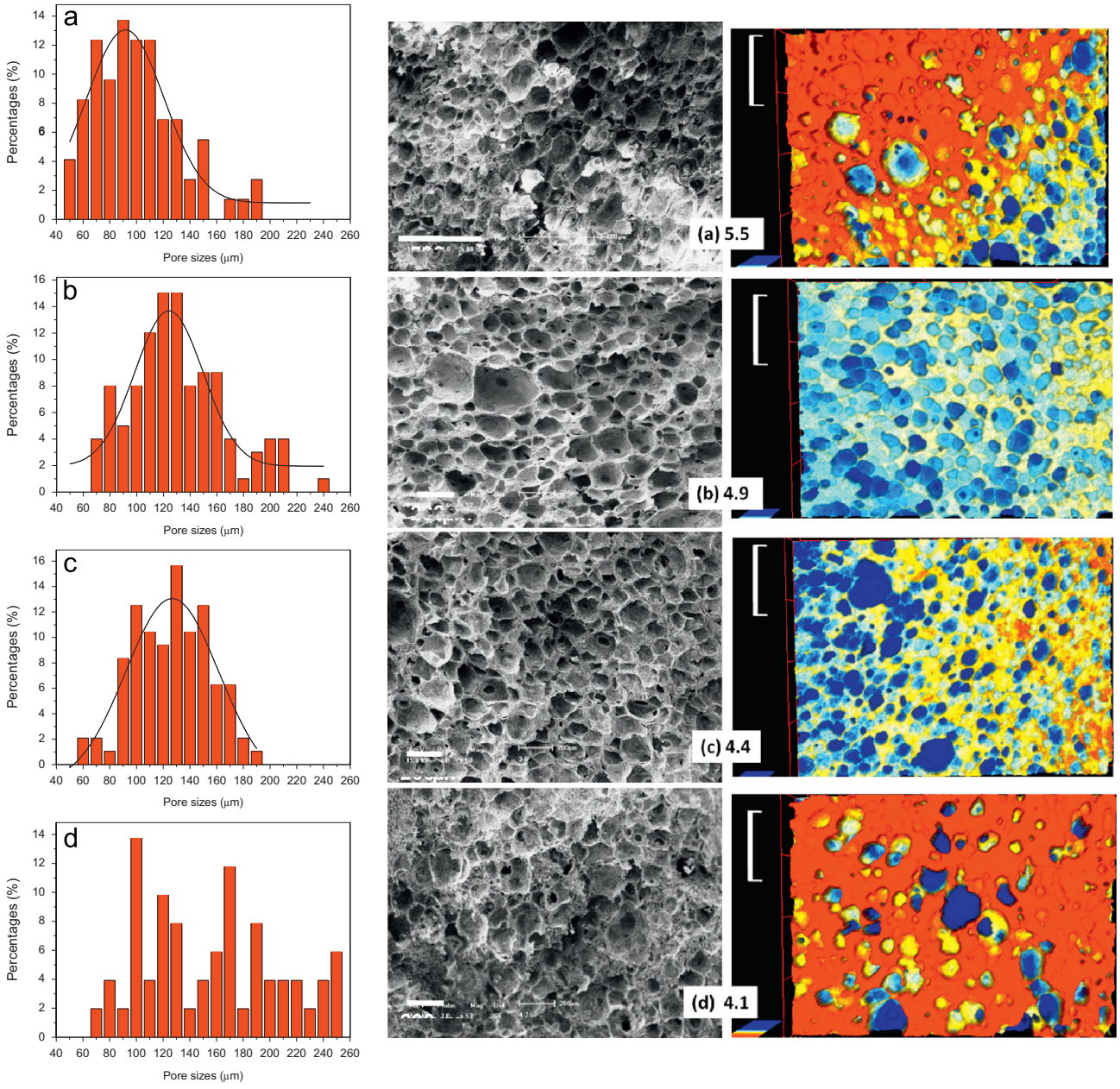

Fig. 2. The macropore size distributions (left column) and SEMs (middle column) and CLSM images (right column) of MHSs by PAF method with different PVA: HA weight ratios: (a) 5.5, (b) 4.9, (c) 4.4 and (d) 4.1. The bars in CLSM images are 510 μm. The macropore size distributions are calculated based on the statistic results of the pore size shown in the SEM images.

Data). Both the dried HA/PVA composite and sintered MHS are machinable (Fig. S2, Supplementary Data). According to our knowledge, this is the first example showing that 3D interconnected MHS can be fabricated based on this mechanism. This pore forming mechanism described above is also different from those employed for the direct freezing the HA aqueous suspension [35–37] or macroporous PVA/HA composite [38–40] in terms of both the preparation protocol and resultant macrostructures. In these reports, the ice crystals induced by the freezing serve as template, while in our protocol, air bubbles instead play the role.

According to the SEM results of MHSs sintered at 1250 °C (Fig. 3a), HA particles in the walls were joined together by sintering, which are reflected by both the interconnection between particles and growth of discrete HA crystals. Single particle with size up to 3 μm can be seen. These results are corroborated by the XRD patterns of MHS sintered at 1250 °C. Compared with the XRD pattern of original HA powders (Fig. 1b), more resolved XRD peaks (Fig. 3b) indicate the growth of the HA crystals. No apparent decomposition of HA during the sintering can be identified based on XRD result. The wall thickness is in the range of 3–10 μm. There are also some sub-micrometer sized pores in the walls, which arise from the decomposition of the PVA and are not eliminated by the sintering.

By varying the weight ratios of PVA/HA, it is demonstrated that the MHSs can be obtained with macropores sizes ranging

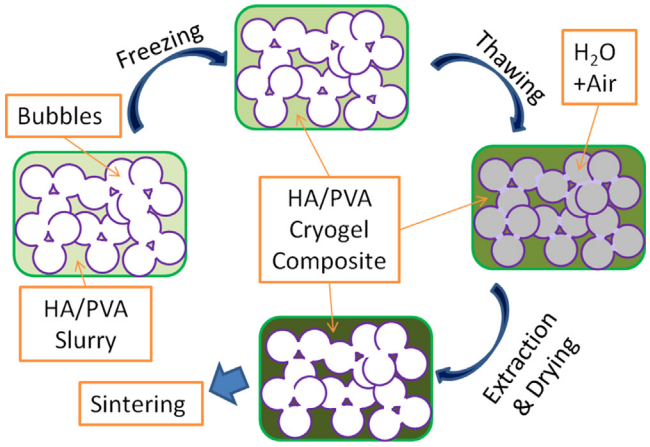

Scheme 1. Schematic of the pore forming mechanism in the PAF method.

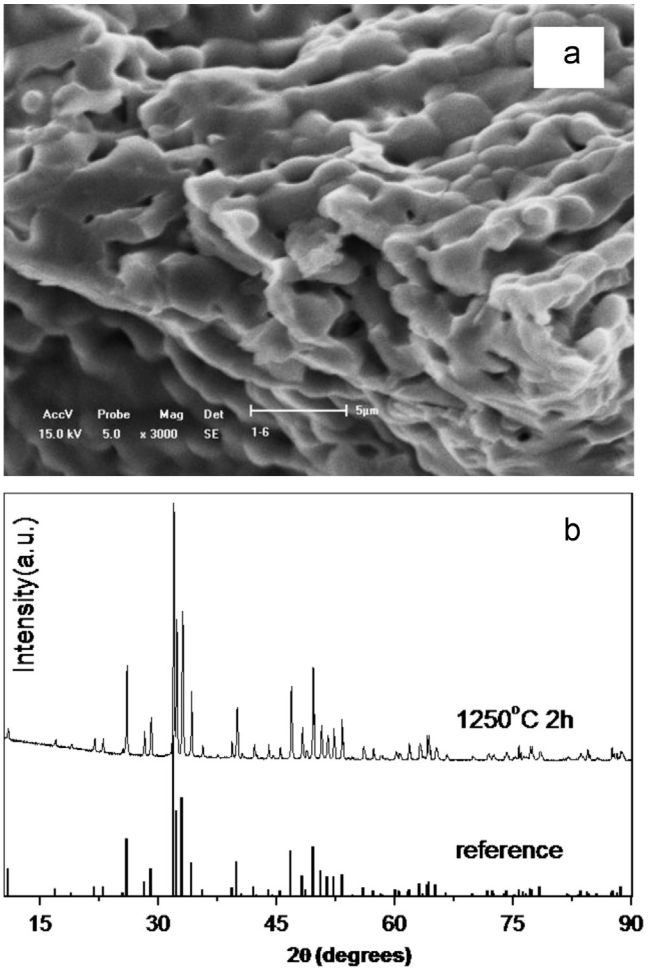

Fig. 3. SEM image (a) and XRD pattern (b) of PAF5.5. Reference pattern was also given for comparison (JCPDS 084-1998).

from 90 to 130 μm with 20–70 μm window pores. Actually, the macropore sizes can be further enlarged by extra mechanical stirring the slurry after bubble incorporation by shaking. Fig. 4 shows the SEM images of MHSs with extra stirring at 1200 rpm. Compared with MHSs prepared without extra stirring (Fig. 2), larger primary macropores in PAF4.9-R and PAF5.5-R ranging from 150 to 200 μm can be observed. The window pores can also be enlarged to around 100 μm. Careful examination of the macropore shapes without (Fig. 2) and with stirring (Fig. 4), the round/near-round shaped macropores change into irregularly shaped larger macropores. This phenomenon arises from the strong shearing force during the vigorous stirring, which stretches walls and merges the bubbles. This can be seen from the very thin walls (Fig. 4, inset) of 1–2 μm. Apparently, the PAF method coupling with extra mechanical stirring at high speed leads to the formation of larger macropores and larger window pore as well. *Via* the PAF method, both the macropores and window pores in these MHSs with or without extra stirring meet the requirement in the pore size defined by application for bone tissue engineering [16–18].

In above sections, the MHSs were all prepared using pure PVA aqueous solution and without using any surfactant. In

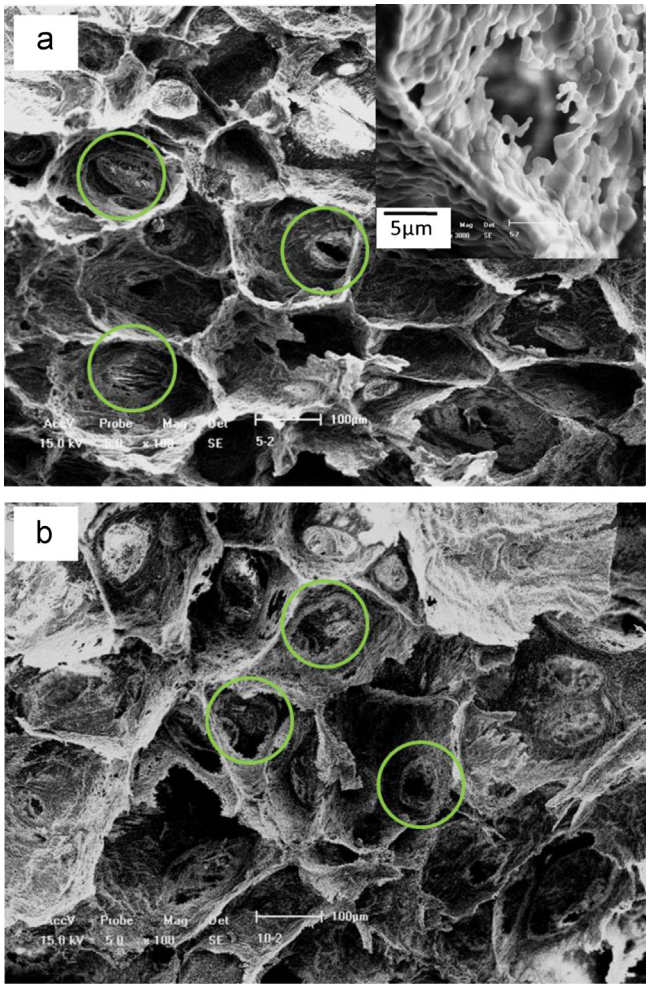

Fig. 4. SEM images of MHSs with extra stirring at 1200 rpm for 10 min and PVA:HA weight of (a) 4.9 and (b) 5.5. Some big window pores are circled for clarity. Inset in (a) shows the sintered walls and presence of smaller window pores.

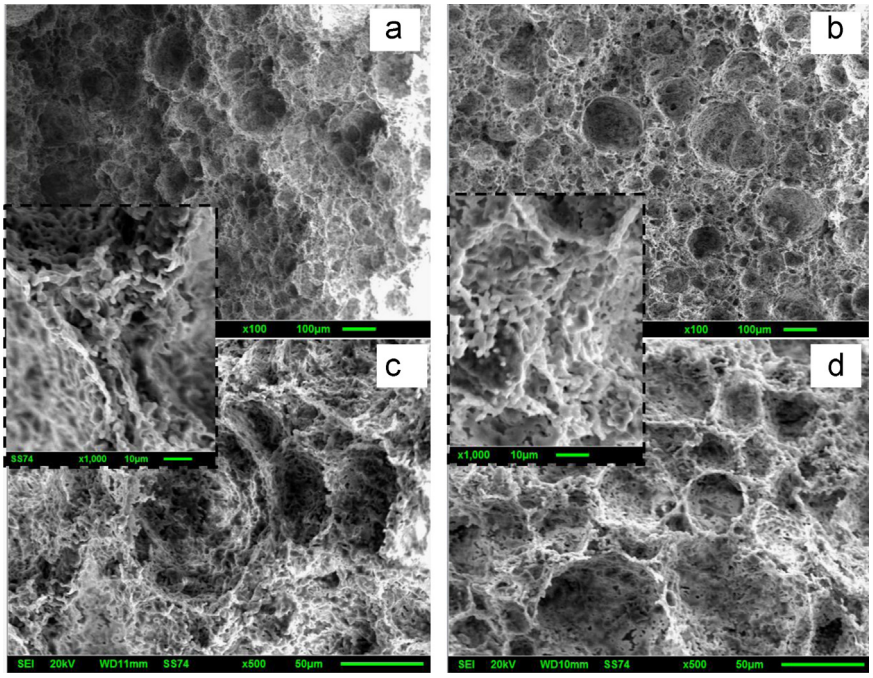

Fig. 5. SEM images of MHSs (PVA:HA=4.9) with SDS of (a–b) 0.7‰ and (c–d) 1.4‰. The insets show the porous walls.

some literatures, surfactants were used as foaming agents to assist the formation of slurries with bubbles [19–22]. In this work, the effect of the surfactant, *i.e.* SDS, on the PAF method derived macrostructures was studied. In Fig. 5, the utilization of the SDS gives rise to much smaller macropore sizes than MHSs prepared by the PAF method without using SDS (Figs. 2 and 4). The decreased macropore sizes upon the addition of SDS can be attributed to the emulsifying effect of SDS, which decreases the surface tension force and thus leads to the formation of smaller air bubbles. The addition of increasing amounts of SDS further leads to slightly decreased macropores sizes. The macropores size of PAF4.9-S0.7 is around 30 μm, while only about 20 μm sized macropore can be obtained for PAF4.9-S1.4 using doubled amount of SDS (1.4‰). Additionally, some sporadic large macropores can also be seen, which are due to the encapsulated larger air bubble and are observable in both cases (PAF4.9-S0.7&1.4). In the SEM images at high magnifications (Fig. 5b and d, × 500), although the sintering behaviors are similar (Fig. 5, insets), it is unable to see the presence of relative large window pores. The primary macropores are indeed connected by the smaller macropores between the sintered HA grains (Fig. 5, insets), which are in contrast with the much more dense walls of MHSs but much larger window pores in the cases without using SDS (Figs. 2 and 4). This observation of the less-densified wall has also been reported by other groups in the presence of surfactants [20,21], which is associated with the different packing behaviors of HA particles. Although the PAF method shows to decrease the macropore size by using small amounts of SDS, such small macropore sizes fall out the optimal pore range shown in the Introduction (50–400 μm) [16–18]. These small macropores might be not advantageous

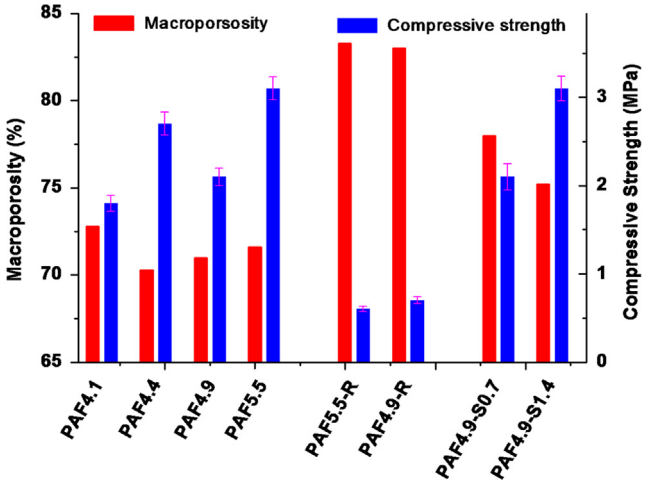

Fig. 6. Macroporosity and corresponding compressive strength of MHSs prepared by PAF method.

to the cell migration and bone ingrowth in these scaffolds. The influence of SDS on the macroporous structures was also reflected in samples prepared using 4.4 wt% PVA solution (PVA:HA=3:3) (Fig. S3, Supplementary Data). Upon the addition of the SDS, comparable macropore sizes can be obtained, which slightly decrease from ~30 μm to ~20 μm when the concentrations of SDS in the PVA solution were increased from 1.2‰ to 2.3‰. Less densified walls still form.

3.3. Macroporosity and compressive strength

The above work shows that the PAF method can produce MHSs with interconnecting pores in the optimal pore range. The

macroporosities of these MHSs were present in the column chart of Fig. 6, in which the compressive strength on the MHSs prepared by the PAF method was also included. Not surprisingly, the compressive strength decreases with the increasing macroporosity. For example, the MHSs with higher macroporosities (~83% for both PAF-4.9R and PAF-5.5R, ~0.7 MPa) show much lower compressive strength than those of the PAF-4.1 ~PAF-5.5 (1.8–3.1 MPa), in which macroporosities range from 70% to 73%. The medium macroporosities in PAF-4.9S series show medium compressive strength. The decreased compressive strength upon high macroporosity is related to the reduced quantity of the solid HA in the specimen. Such dependence of the compressive strength on the macroporosity has also been reported elsewhere [20,41]. It is worthy to mention that the compressive strength for MHSs developed in this work is comparable to those with similar macrostructures [20,21,30,42]. It is known that the highly porous structures are advantageous to the osteoconduction and bone ingrowth. In PAF-4.1 ~PAF-5.5 series, the obtained high macroporosities (70–73%) and compressive strength of 1.8–3.1 MPa represent a good balance for bone tissue engineering applications. Such strength is comparable to the low end of compressive strength of cancellous bone (2–25 MPa) [43,44] and ISO standard [45]. It is thus reasonable to expect that the mechanical property of such MHSs, when implanted and cultured *in vivo*, will increase with the continuous formation of new bone tissue.

4. Conclusion

It is demonstrated in this work that *via* a simple PVA assisted foaming method (PAF method), the 3D interconnected macroporous hydroxyapatite scaffolds can be prepared without using porogens or templates or chemical process. Uniform and tunable macropore sizes (90–130 μm) with window pore size ranging from 20 to 70 μm can be facilely achieved. Well balanced macroporosity (70–73%) with the compressive strength (1.8–3.1 Mpa) can be obtained by this method. With the help of extra mechanical stirring to the agitation, the macropore sizes can be further enlarged to 150–200 μm at the sacrifice of the compressive strength (< 1 Mpa). These sizes of MHSs fall in the optimal pore range proposed for the bone tissue engineering application. By contrast, the addition of small amounts of surfactant (SDS) to the preparation mixture leads to significant decreases in the macropore sizes to 20–30 μm.

Acknowledgment

This work was supported by Project supported by the State Key Program of National Natural Science of China (Grant no. 51032007) and the National Natural Science Foundation of China (Grant nos. 21201030, 51272039), and also the Fundamental Research Funds for the Central Universities (N120410001 and N100702001).

Appendix A. Supporting information

Supplementary data associated with this article can be found in the online version at http://10.1016/j.ceramint.2013.07.079.

References

[1] R.M. Pilliar, M.J. Filiaggi, J.D. Wells, M.D. Grynpas, R.A. Kandel, Porous calcium polyphosphate scaffolds for bone substitute applications—in vitro characterization, Biomaterials 22 (2001) 963–972.
[2] R.W. Bucholz, A. Carlton, R.E. Holmes, Hydroxyapatite and tricalcium phosphate bone graft substitutes, Orthopedic Clinics of North America 18 (1987) 323–334.
[3] P. Ducheyne, Q. Qiu, Bioactive ceramics: the effect of surface reactivity on bone formation and bone cell function, Biomaterials 20 (1999) 2287–2303.
[4] V. Karageorgiou, D. Kaplan, Porosity of 3D biomaterial scaffolds and osteogenesis, Biomaterials 26 (2005) 5474–5491.
[5] Y. Gonda, K. Ioku, Y. Shibata, T. Okuda, G. Kawachi, M. Kamitakahara, H. Murayama, K. Hideshima, S. Kamihira, I. Yonezawa, H. Kurosawa, T. Ikeda, Stimulatory effect of hydrothermally synthesized biodegradable hydroxyapatite granules on osteogenesis and direct association with osteoclasts, Biomaterials 30 (2009) 4390–4400.
[6] Q. Chang, D.L. Chen, H.Q. Ru, X.Y. Yue, L. Yu, C.P. Zhang, Toughening mechanisms in iron-containing hydroxyapatite/titanium composites, Biomaterials 31 (2010) 1493–1501.
[7] A.E. Porter, N. Patel, J.N. Skepper, S.M. Best, W. Bonfield, Comparison of in vivo dissolution processes in hydroxyapatite and silicon-substituted hydroxyapatite bioceramics, Biomaterials 24 (2003) 4609–4620.
[8] E. Chevalier, D. Chulia, C. Pouget, M. Viana, Fabrication of porous substrates: a review of processes using pore forming agents in the biomaterial field, Journal of Pharmaceutical Sciences 97 (2007) 1135–1153.
[9] B. Baroli, From Natural bone grafts to Tissue engineering therapeutics: brainstorming on pharmaceutical formulative requirements and challenges, Journal of Pharmaceutical Sciences 98 (2009) 1174–1317.
[10] M.P. Ginebra, M. Espanol, E.B. Montufar, R.A. Perez, G. Mestres, New processing approaches in calcium phosphate cements and their applications in regenerative medicine, Acta Biomaterialia 6 (2010) 2863–2873.
[11] P.S. Eggli, W. Muller, R.K. Schenk, Porous hydroxyapatite and tricalcium phosphate cylinders with two different pore size ranges implanted in the cancellous bone of rabbits, Clinical Orthopaedics and Related Research 232 (1988) 127–138.
[12] A.I. Itala, H.O. Ylanen, C. Ekholm, K.H. Karlsson, H.T. Aro, Pore diameter of more than 100 μm is not requisite for bone ingrowth in rabbits, Journal of Biomedical Materials Research 58 (2001) 679–683.
[13] K. Shimazaki, V. Mooney, Comparative study of porous hydroxyapatite and tricalcium phosphate as bone substitute, Journal of Orthopaedic Research 3 (1985) 301–310.
[14] R.E. Holmes, R.W. Bucholz, V. Mooney, Porous hydroxyapatite as a bone graft substitute in diaphyseal defects: a histometric study, Journal of Orthopaedic Research. 5 (1987) 114–121.
[15] G. Daculsi, N. Passuti, Effect of the porosity for osseous substitution of calcium phosphate ceramics, Biomaterials 11 (1990) 86–87.
[16] B.S. Chang, C.K. Lee, K.S. Hong, H.J. Youn, H.S. Ryu, S.S. Chung K.W. Park, Osteoconduction at porous hydroxyapatite with various pore configurations, Biomaterials 21 (2000) 1291–1298.
[17] B. Flautre, M. Descamps, C. Delecourt, M.C. Blary, P. Hardouin, Porous HA ceramic for bone replacement: role of the pores and interconnections—experimental study in the rabbit, Journal of Materials Science: Materials in Medicine 12 (2001) 679–682.
[18] J. Bobyn, R. Pilliar, H. Cameron, G. Weatherly, The optimal pore size for the fixation of porous surfaced metal implants by the ingrowth of bone, Clinical Orthopaedics and Related Research 150 (1980) 263–270.
[19] J.E. Gough, J.R. Jones, L.L. Hench, Nodule formation and mineralisation of human primary osteoblasts cultured on a porous bioactive glass scaffold, Biomaterials 25 (2004) 2039–2046.

[20] E.B. Montufar, T. Traykova, C. Gil, I. Harr, A. Almirall, A. Aguirre, E. Engel, J.A. Planell, M.P. Ginebra, Foamed surfactant solution as a template for self-setting injectable hydroxyapatite scaffolds for bone regeneration, Acta Biomaterialia 6 (2010) 876–885.
[21] L.A. Cyster, D.M. Grant, S.M. Howdle, F.R.A.J. Rose, D.J. Irvine, D. Freeman, C.A. Scotchford, K.M. Shakesheff, The influence of dispersant concentration on the pore morphology of hydroxyapatite ceramics for bone tissue engineering, Biomaterials 26 (2005) 697–702.
[22] P. Sepulveda, J.G.P. Binner, S.O. Rogero, O.Z. Higa, J.C. Bressiani, Production of porous hydroxyapatite by the gel-casting of foams and cytotoxic evaluation, Journal of Biomedical Materials Research 50 (2000) 27–34.
[23] D. Tadic, F. Beckmann, K. Schwarz, M. Epple, A novel method to produce hydroxyapatite objects with interconnecting porosity that avoids sintering, Biomaterials 25 (2004) 3335–3340.
[24] L. Ji, G Jell, Y. Dong, J.R. Jones, M.M. Stevens, Template synthesis of ordered macroporous hydroxyapatite bioceramics, Chemical Communications 47 (2011) 9048–9050.
[25] B.H. Fellah, P. Layrolle, Sol–gel synthesis and characterization of macroporous calcium phosphate bioceramics containing microporosity, Acta Biomaterialia 5 (2009) 735–742.
[26] M. Descamps, O. Richart, P. Hardouin, J.C. Hornez, A. Leriche, Synthesis of macroporous β-tricalcium phosphate with controlled porous architectural, Ceramics International 34 (2008) 1131–1137.
[27] G. Tripathi, B. Basu, A porous hydroxyapatite scaffold for bone tissue engineering: Physico-mechanical and biological evaluations, Ceramics International 38 (2012) 341–349.
[28] J. Zhao, X. Lu, K. Duan, L.Y. Guo, S.B. Zhou, J. Weng, Improving mechanical and biological properties of macroporous HA scaffolds through composite coatings, Colloids Surface B 74 (2009) 159–166.
[29] S. Roohani-Esfahani, S. Nouri-Khorasani, Z. Lu, R. Appleyard, H. Zreiqat, The influence hydroxyapatite nanoparticle shape and size on the properties of biphasic calcium phosphate scaffolds coated with hydroxyapatite-PCL composites, Biomaterials 31 (2010) 5498–5509.
[30] B. Li, X.N. Chen, B. Guo, X.L. Wang, H.S. Fan, X.D. Zhang, Fabrication and cellular biocompatibility of porous carbonated biphasic calcium phosphate ceramics with a nanostructure, Acta Biomaterialia 5 (2009) 134–143.
[31] A. Almirall, G. Larrecq, J.A. Delgado, S. Martínez, J.A. Planell M.P. Ginebra, Fabrication of low temperature macroporous hydroxyapatite scaffolds by foaming and hydrolysis of an a-TCP paste, Biomaterials 25 (2004) 3671–3680.
[32] W. Wang, Q. Chang, B.S. Chu, C.Q. Lin, S. Chen, H.Q. Ru, One kind of fabrication method for macroporous hydroxyapatite, CN Patent no. 201110148091.X (2013).
[33] V.I. Lozinsky, Cryotropic gelation of poly(vinyl alcohol) solutions, Russian Chemical Review 67 (1998) 573–586.
[34] Q. Fu, M.N. Rahaman, F. Dogan, B.S. Bal, Freeze-cast hydroxyapatite scaffolds for bone tissue engineering applications, Biomedical Materials 3 (2008) 89–109.
[35] S. Deville, E. Saiz, A.P. Tomsia, Freeze casting of hydroxyapatite scaffolds for bone tissue engineering, Biomaterials 27 (2006) 5480–5489.
[36] Q. Fu, M.N. Rahaman, F. Dogan, B.S. Bal, Freeze casting of porous hydroxyapatite scaffolds. I. processing and general microstructure, Journal of Biomedical Materials Research Part B Applied Biomaterials 86 (2008) 125–135.
[37] Q. Fu, M.N. Rahaman, F. Dogan, B.S. Bal, Freeze casting of porous hydroxyapatite scaffolds. II. sintering, microstructure, and mechanical behavior, Journal of Biomedical Materials Research Part B Applied Biomaterials 86 (2008) 514–522.
[38] A. Sinha, S. Nayar, A. Kar, M.K. Gunjan, B. Mahato, G. Das, Microhydrogel-mediated synthesis of sintered hydroxyapatite granules, International Journal of Applied Ceramic Technology 5 (2008) 458–463.
[39] K.H. Zuo, Y.P. Zeng, D.L. Jiang, Effect of polyvinyl alcohol additive on the pore structure and morphology of the freeze-cast hydroxyapatite ceramics, Materials Science and Engineering: C 30 (2010) 283–287.
[40] A. Sinha, A. Guha, Biomimetic patterning of polymer hydrogels with hydroxyapatite nanoparticles, Materials Science and Engineering: C 29 (2009) 1330–1333.
[41] J.C. Le Huec, T. Schaeverbeke, D. Clement, J. Faber, A. Le Rebeller, Influence of porosity on the mechanical resistance of hydroxyapatite ceramics under compressive stress, Biomaterials 16 (1995) 113–118.
[42] D.M. Liu, Influence of porosity and pore size on the compressive strength of porous hydroxyapatite ceramic, Ceramics International 23 (1997) 135–139.
[43] F.G. Evans, A. King, Regional differences in some physical properties of human spongy bone. In: biomechanical Studies of the Musculo-Skeletal System, Springfield: Thomas (1961) 19–67.
[44] A Odgaard, F. Linde, The underestimation of Young's modulus in compressive testing of cancellous bone specimen, Journal of Biomechanics 8 (1991) 691–698.
[45] Implants for surgery-hydroxyapatite. Part1. Ceramic hydroxyapatite BS, ISO 13779-1:2000.